Proceedings of the ASME 2017 International Design Engineering Technical Conferences & Computers and Information in Engineering Conference
IDETC2017
August 6-9, 2017, Cleveland, Ohio, USA

DETC2017/MSNDC-67937

COMPARISON OF CONTROL METHODS FOR TWO-LINK PLANAR FLEXIBLE MANIPULATOR *

Joseph Bowkett†
Jet Propulsion Laboratory
California Institute of Technology
Pasadena California 91109
jbowkett@caltech.edu

Rudranarayan Mukherjee
Jet Propulsion Laboratory
California Institute of Technology
Pasadena California 91109
Rudranarayan.M.Mukherjee@jpl.nasa.gov

ABSTRACT

While the majority of terrestrial multi-link manipulators can be considered in a purely kinematic sense due to their high stiffness, the launch mass restrictions of aerospace applications such as in-orbit assembly of large space structures result in low stiffness links being employed, meaning dynamics can no longer be ignored. This paper seeks to investigate the suitability of several different open and closed loop control techniques for application to the problem of end effector position control with minimal vibration for a low stiffness space based manipulator. Simulations of a representative planar problem with two flexible links are used to measure performance and sensitivity to parameter variation of: model predictive control, command shaping, and command shaping with linear quadratic regulator (LQR) feedback. An experimental testbed is then used to validate simulation results for the recommended command shaped controller.

BACKGROUND

Designs for space-based technologies are becoming ever more ambitious as new and more inventive applications are conceived. Space-based solar power offers the prospect of higher energy collection rates, constant exposure, and increased longevity compared to ground based plants [1], while large aperture telescopes offer astronomers the prospect of directly imaging distant celestial bodies such as exoplanets [2].

In other work [3], the authors and their collaborators are also investigating the technology required to realize such structures through the In-Space Telescope Assembly Robotics project. A multi-limbed robot is used to construct a large truss out of collapsible modules by employing the same end effectors to both place new modules and move over the existing structure. Individual mirror modules are then attached to the support truss by the assembly robot to form the segmented primary mirror.

One problem aspect of particular interest is the possibility of vibration being excited in both the robot's limbs and the supporting structure, as launch mass requirements results in these being highly flexible (much like the Space Shuttle's Canadarm) when compared to terrestrial equivalents [4]. The facet of the problem being addressed in this paper is point to point motion of an end effector in free space, prior to grasping a truss module. Path planning cannot be achieved purely through inverse kinematics as the compliance of the long links that form the manipulator mean dynamics cannot be neglected.

The arm will be required to handle both truss and mirror modules (being of different mass), and the stiffness of the underlying structure will change as modules are added, which will require development of controllers robust to variations in system parameters. For this purpose a simulation of a two-link planar flexible arm under the effect of gravity (seen in Fig. 1) has been used to investigate the performance and sensitivity of several control methods. The 'truth' dynamics of the MATLAB simulations employ a divide and conquer algorithm applied to an

†Corresponding author

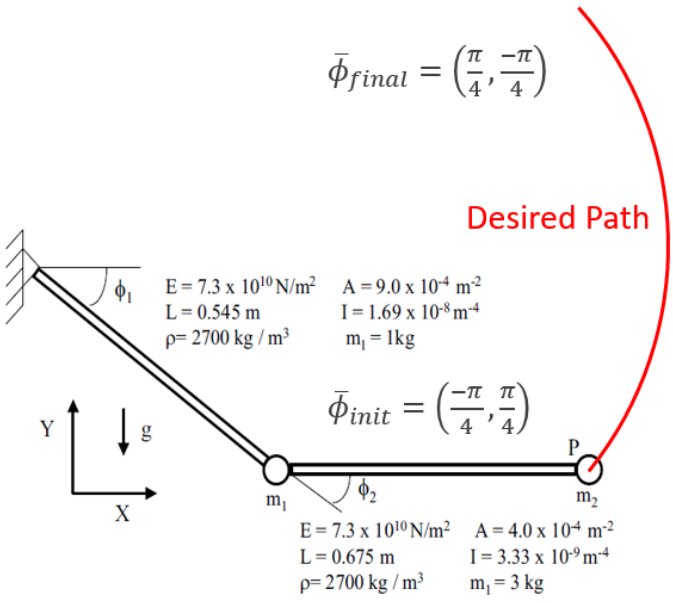

FIGURE 1: TWO-LINK FLEXIBLE MANIPULATOR [5]

assumed mode method furnished by Mukherjee et al. [5]. Joint angles are commanded to move through $\pi/2$ radians in opposite directions which preserves the horizontal orientation of the second link.

While single-link manipulators can be considered with a linearized model, this is not true for multi-link manipulators, as mode shapes vary as a function of configuration [6]. A range of different techniques have been used to analyse the dynamics of flexible multi-link manipulators including finite element methods [7], lumped parameter models [8], and the assumed mode method, which is most widely used for single flexible links [9]. While mode shapes can be determined through extensive simulation or experiment results [10], complexity of the assumed mode method grows with degrees of freedom [11], and as it is desired to generalize these controllers to more than two flexible links the lumped parameter method was selected for computational efficiency.

MODEL PREDICTIVE CONTROL

Model predictive control (MPC) was originally developed for slow moving production processes in the chemical engineering industry, but with advances in processing speed has now been adopted across a variety of disciplines including flexible manipulators [12]. Boscariol et al. apply MPC to a simulated flexible four-bar linkage using a linearized plant model, with a finite-element model providing 'truth' dynamics [13]. While they show improved position tracking and vibration suppression compared to standard PID control, the results from their closed chain mechanism may not generalize to open chain manipulators due to only having a single kinematic constraint at the base of the chain.

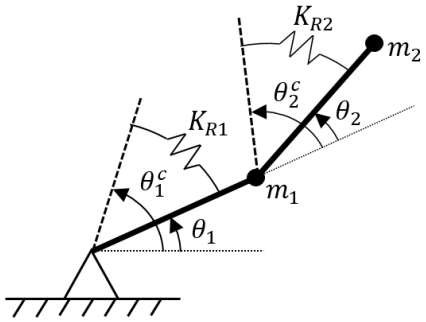

FIGURE 2: LUMPED PARAMETER MODEL
θ_i^c: Applied joint angle K_{Ri}: Effective series elasticity
θ_i: Angle of equivalent rigid link

A model predictive controller was therefore developed to investigate performance and robustness for flexible link open chain manipulators. The flexible dynamics were simplified into a lumped parameter model as seen in Fig. 2 which was then linearized at the beginning of each prediction window. Compliance of each joint/link pair was grouped into a single series elasticity between the commanded joint angle and an idealized rigid link. This relied on small angle approximations which were found to hold for all stable controllers. The dynamics of the lumped parameter model were derived with Lagrangian mechanics with Eq. 1 and Eq. 2 representing torque about the first and second joints respectively.

$$T_1 = [(m_1+m_2)L_1^2 + m_2L_2^2 + m_2L_1L_2cos(\theta_2)]\ddot{\theta}_1 + [m_2L_2^2 + m_2L_1L_2cos(\theta_2)]\ddot{\theta}_2 - K_{R1}(\theta_1^C - \theta_1) + (m_1+m_2)gL_1cos(\theta_1) + m_2gL_2cos(\theta_1+\theta_2) - m_2L_1L_2sin(\theta_2)(2\dot{\theta}_1\dot{\theta}_2 + \dot{\theta}_2^2) \quad (1)$$

$$T_2 = [m_2L_2^2 + m_2L_1L_2cos(\theta_2)]\ddot{\theta}_1 + m_2L_2^2\ddot{\theta}_2 + m_2L_1L_2sin(\theta_2)\dot{\theta}_1^2 + m_2gL_2cos(\theta_1+\theta_2) - K_{R2}(\theta_2^C - \theta_2) \quad (2)$$

Controller Performance After initial tuning the MPC proved capable of smooth motion between the initial and desired final end effector locations as seen in Fig. 3. An open loop cubic polynomial trajectory provides a reference for comparison, the response for which over a 1.5 second motion is seen in black. The red line denotes the end effector position if the cubic polynomial were applied to a perfectly rigid arm. The response to the tuned MPC controller can be seen in blue, which employs a prediction horizon of 500ms across a discretization of 4ms, an execution time of 100ms, state error weighting of 100 and control weighting of 1.

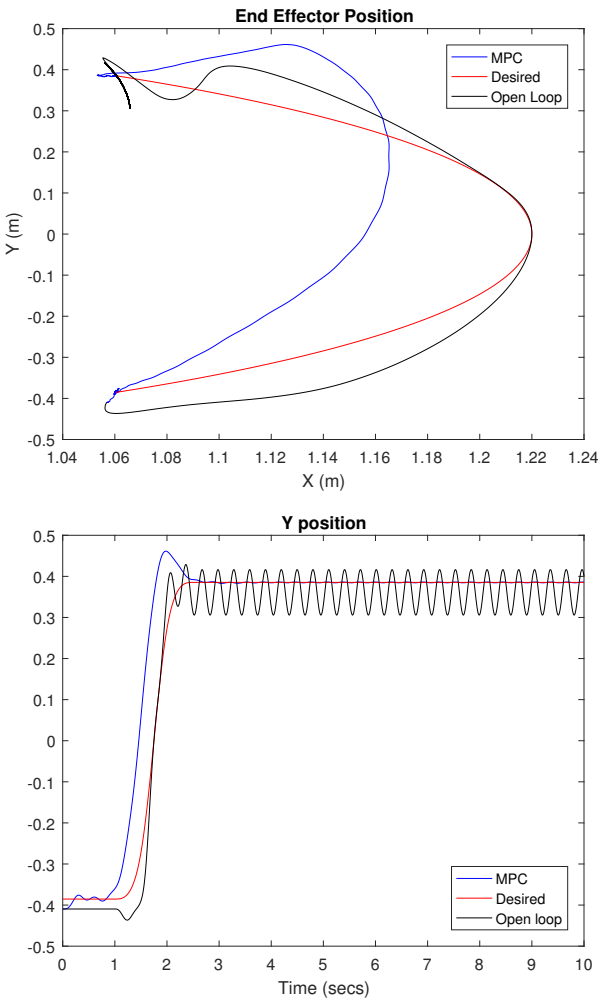

FIGURE 3: OPEN LOOP CUBIC TRAJECTORY AND MODEL PREDICTIVE CONTROL RESPONSE
TOP: PATH OF END EFFECTOR LOCATION IN CARTESIAN SPACE, BOTTOM: TIME HISTORY OF VERTICAL POSITION

While the MPC introduces a slight overshoot not seen with the open loop response, it damps residual vibrations rapidly at the end of the motion and brings the end effector to the desired location. By contrast the response to the cubic polynomial has considerable residual vibration, the mean position for which is below that of the desired end effector location due to the steady state error introduced by gravity.

Sensitivity In order to determine the sensitivity of the controller to inaccuracies in the system model, the parameters of the underlying 'truth' assumed mode method were varied by

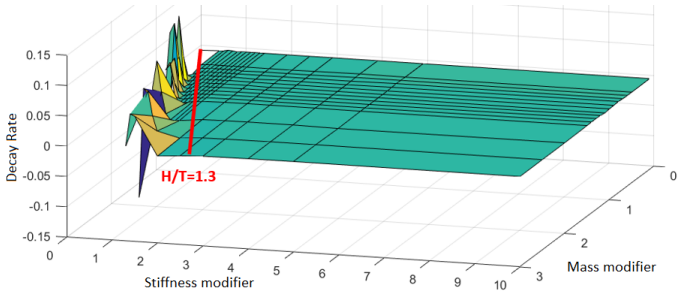

FIGURE 4: VIBRATION DECAY RATE AS FUNCTION OF STIFFNESS AND MASS MODIFIER
H: Uncontrolled natural period, T: Prediction horizon = 500ms

application of linear modifiers to the stiffness and mass, while keeping the parameters within the simplified model used for prediction fixed.

A sweep of 4096 simulations was used to determine the influence of these parameters along with that of the prediction and execution horizons employed by the MPC. Across results where the controller was stable the overshoot remained largely the same, while settling time for the damping of residual vibration increased slightly with a disparity in stiffness or mass. No steady state error was introduced as the end effector position was the only weighted state in the MPC formulation.

The more interesting result came from the boundary at which the controller became unstable. As seen in Fig. 4, when there were less than 1.3 natural periods of the system in the final configuration within the prediction horizon of the controller the decay rate of the residual vibration was positive. This hints at a phenomenon similar to the Nyquist criterion where more than one period of a mode must be predicted for the controller to be able to compensate for it.

COMMAND SHAPING

Since its initial proposal for use on the Space Shuttle's Canadarm [14], input shaping or command shaping has seen wide adoption in open loop path planning for flexible systems. It has seen successful application to single link flexible manipulators [15] when vibratory modes are static, but can be difficult to generalize to multi-link systems as the mode shapes and frequencies (which determine the spacing of impulses used to cancel residual vibration) vary as a function of configuration [16].

Romano et al. empirically compared the performance of command shaping with that of a smoothed bang-bang reference signal, for one and two flexible link arms on a gravity offset testbed [17]. They concluded that while smoothed bang-bang control was capable of producing good tracking with a single flexible link, only the command shaped input was able to produce point to point motion with minimal vibration when both

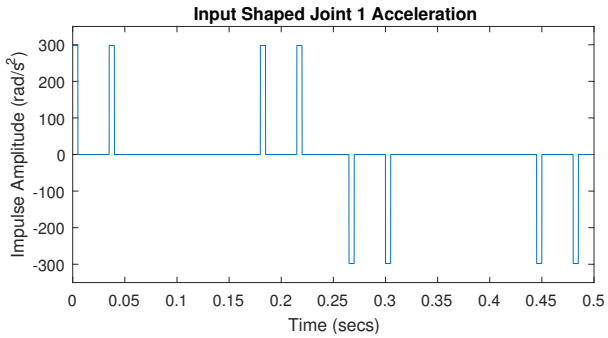

FIGURE 5: COMMAND SHAPED ACCELERATION PROFILE OF FIRST JOINT

links were flexible.

Khorrami et al. implemented a nonlinear inner-loop controller to reduce variations in natural frequencies due to the configuration of multi-link flexible manipulators, in order to improve response to shaped commands [18]. Experiments were conducted on a similar testbed to those of Romano, and demonstrated the ability of the controller to correct for variations in payload which modify the natural period of the manipulator and therefore the impulse spacing.

While a wide range of advancements have been made in the field of command shaping [19], the intent of this paper is to compare the original open loop technique with the performance of MPC using a linearized model on the same system.

Performance Fig. 5 shows the command shaped acceleration profile applied to the first joint, which has the effect of canceling residual vibrations from the first two modes when properly calibrated from prior measurements of the natural period at each configuration. While the speed of motion with the linearized MPC technique was limited by the overshoot of the feedback controller, command shaping permitted much more rapid changes of angle. The performance of the technique was therefore evaluated against the same open loop cubic polynomial but over a 0.5 second trajectory, the response to which can be seen in black in Fig. 6. The amplitude of the residual vibration from the naive open loop motion increases considerably with the threefold increase in speed of the motion.

The response of the system to the command shaped accelerations can be seen in blue, with minimal residual vibration despite the rapid motion of each joint. The properly tuned response also places the end effector precisely on the desired location. With a perfect system model and accurate knowledge of the stiffness and mass of each component we are therefore able to demonstrate the ideal characteristics for the response.

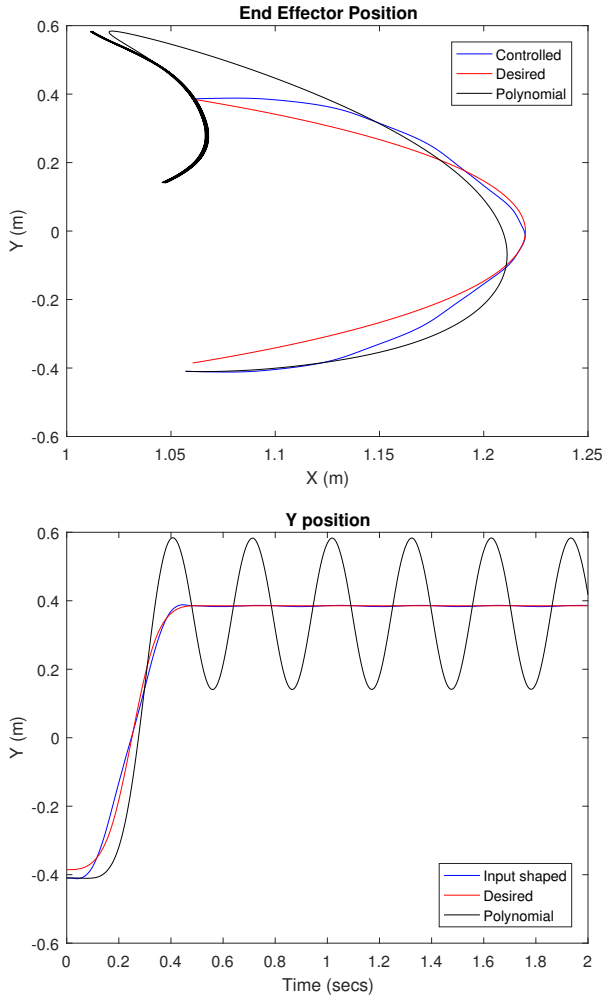

FIGURE 6: OPEN LOOP CUBIC TRAJECTORY AND TUNED SHAPE COMMAND RESPONSE
TOP: PATH OF END EFFECTOR LOCATION IN CARTESIAN SPACE, BOTTOM: TIME HISTORY OF VERTICAL POSITION

Sensitivity In the same manner as for MPC the sensitivity of the input shaping technique was investigated by keeping controller parameters fixed (pulse amplitude and separation) while varying parameters of the 'truth' model in simulation. Figure 7 shows the response of the system when tuned to the original parameters if the mass of all system components is reduced by 20%. As the natural period of the system has changed the responses to each of the pulses shift out of phase and are no longer entirely cancelled.

One method of increasing the robustness of the command shaping technique to parameter variations is that of a 'Zero Vibration and Derivative' form [19]. This employs three or more

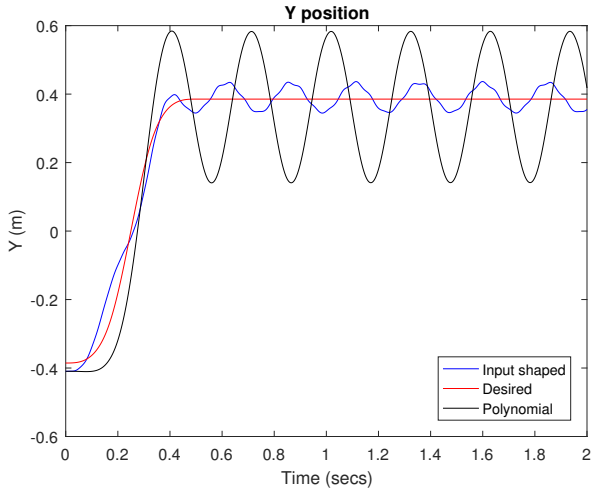

FIGURE 7: VERTICAL POSITION OF END EFFECTOR WITH MASS DECREASED ACROSS ALL SYSTEM COMPONENTS BY 20%

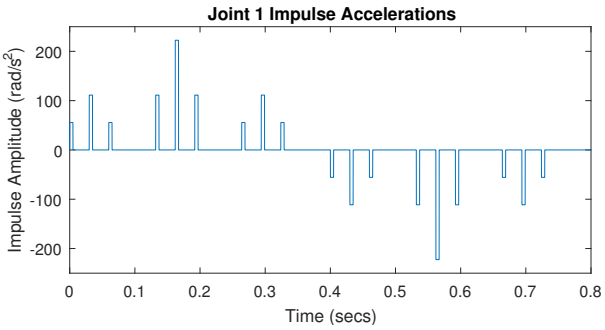

FIGURE 8: 'ZERO VIBRATION DERIVATIVE' ACCELERATION PROFILE, THREE IMPULSES CONVOLVED OVER TWO MODES

impulses which has the effect of reducing the derivative of residual vibration, as a function of predicted frequency over true natural frequency, to zero. While this is an improvement over the two impulse response it has the drawback of requiring at least 1.5 natural periods of the first mode of the system for all acceleration and deceleration profiles, the duration for which is longer than the 0.5 second motion previously demonstrated.

In order to determine the benefit of applying a ZVD shaper to the system simulations were conducted over the same trajectory with a 0.75 second duration. The impulse accelerations for the ZVD shaper can be seen in Fig. 8; the improvement in robustness between two and three pulses per mode can be seen in Fig. 9.

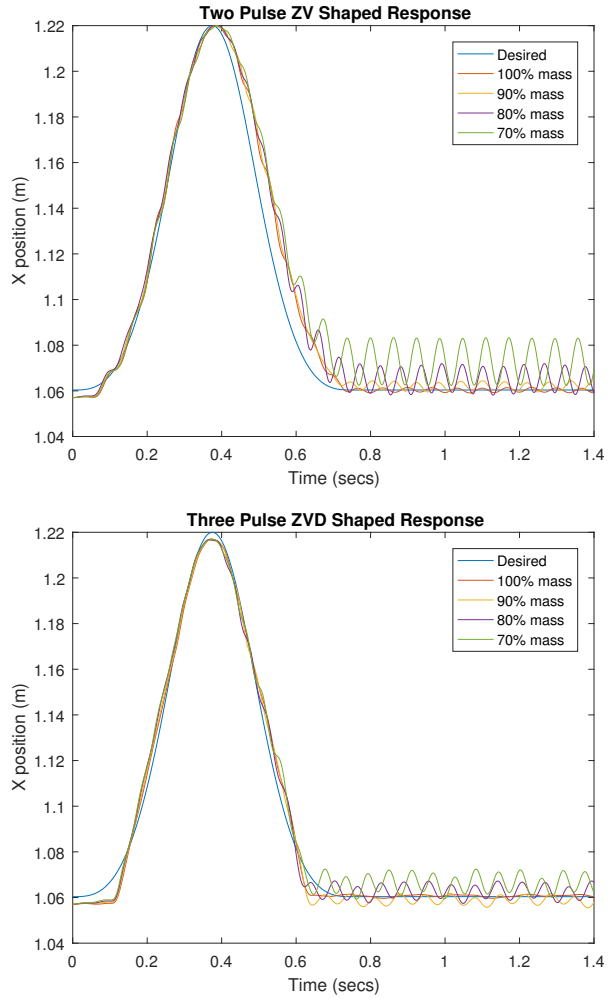

FIGURE 9: END EFFECTOR RESPONSE IN X DIRECTION TO OPEN LOOP COMMAND SHAPING WITH TWO AND THREE ACCELERATION PULSES PER FREQUENCY DEMONSTRATING INCREASED ROBUSTNESS TO MASS VARIATION

COMMAND SHAPING WITH LQR

While the robustness of the command shaping method can be increased with additional impulses, a moderate change in system parameters still results in a considerable increase in residual vibration and mean position error. To further improve robustness a linear quadratic regulator (LQR) feedback controller was applied to the system after the prescribed open loop motion, which employed full state feedback to asymptotically stabilize the effective rigid joint angles. The plant model in the LQR formulation was taken as the linearization of the lumped parameter model about the desired final configuration. The control to be minimized in the LQR cost function was the acceleration of the

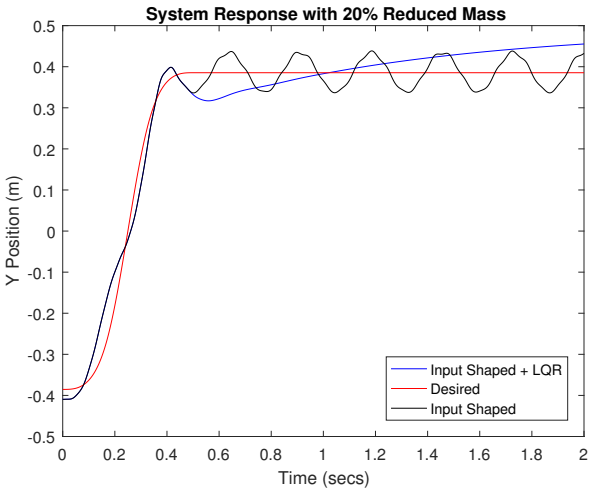

FIGURE 10: VERTICAL POSITION OF END EFFECTOR WITH MASS DECREASED ACROSS ALL SYSTEM COMPONENTS BY 20%, WITH AND WITHOUT FEEDBACK CONTROL

applied joint angles so as to represent dynamic torque, with cost coefficients for state error of $q = 100$ and control effort of $r = 1$.

The addition of feedback control has little to no effect on the system response with original parameters as expected, given the open loop trajectory had already been tuned to produce the desired tracking performance. The combined control is very effective at damping residual vibrations caused by parameter variation, as seen in Fig. 10. However, as the coefficients for the LQR state feedback are derived from the system model with incorrect parameters, there is a steady state error introduced to the output state of end effector position. This could be accounted for through application of online system ID to adapt the state feedback coefficients in response to an observed change in the system output.

EXPERIMENTAL WORK

A representative experimental testbed was constructed to validate the simulated results using command shaping of the joint velocity profile, as seen in Fig. 11. Actuation and sensing are provided by three Hebi X5-4 motors, which contain an IMU and torque transducer as well as a series elastic gearing. Two motors act as joints while the third motor at the end effector provides purely a tip mass and sensing. This produces the system seen in Fig. 12, where both joints and links contribute to manipulator compliance. Extending the lumped parameter method used in simulation allows summing the effective compliance of each link with its respective joint to produce a simplified model.

Series elasticity in the Hebi actuator gearing was found empirically to be 13Nm/rad. The aluminum links are of dimensions 300x30x3.175mm giving a moment of inertia of $I = 80mm^4$ which with a Young's modulus of $E = 70GPa$ equates to an approximate lumped parameter stiffness of 622Nm/rad. The combination of these two series elasticities therefore produces 12.7Nm/rad of compliance in each joint of the simplified lumped parameter model. Each Hebi actuator weighs 335g.

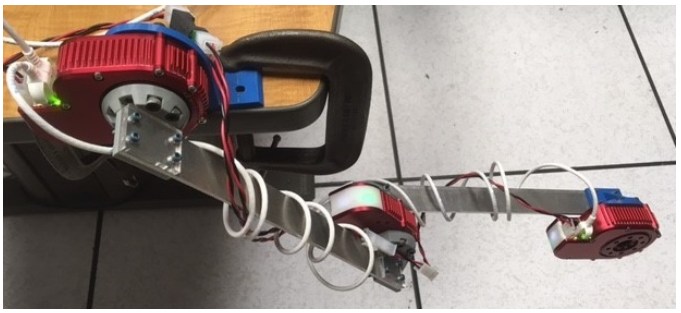

FIGURE 11: TWO-LINK FLEXIBLE MANIPULATOR TESTBED CONSTRUCTED OF HEBI X5 ACTUATORS EACH WITH INTERNAL IMU, CONNECTED BY THIN FLEXIBLE ALUMINUM LINKS

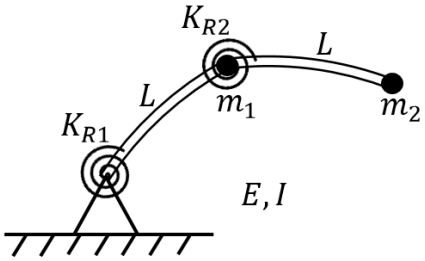

FIGURE 12: SYSTEM MODEL WITH COMPLIANCE IN BOTH JOINTS AND LINKS, WITH TIP MASS ON EACH LINK

Control Methodology The Hebi X5 motors are monitored and controlled over a TCP/IP connection with a controlling computer, with a range of APIs available for different languages. This experiment employed C++ on an Ubuntu 16.04 machine in an effort to minimize processing time and increase command update rate. Each actuator could be set to a desired position, velocity, or output torque with selectable gains for each controller. Direct control of the motor PWM was also possible, however, the latency of the TCP/IP connection lead to velocity controllers designed on the control PC to supply PWM commands having fragile stability at best. For this reason the inbuilt Hebi velocity command was used to apply acceleration impulses as step

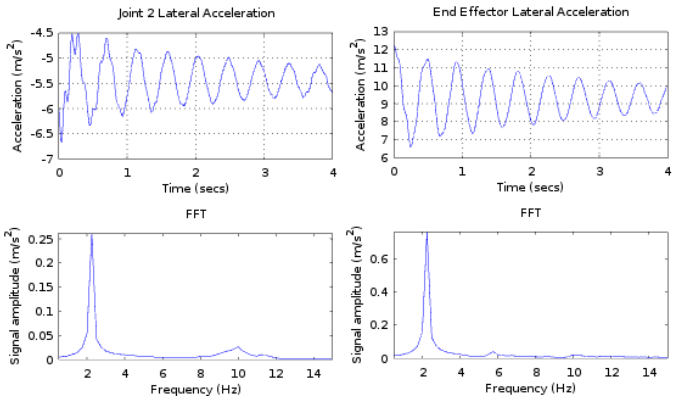

FIGURE 13: LATERAL ACCELERATION AND FAST FOURIER TRANSFORM OF RESIDUAL VIBRATION FOR INITIAL MANIPULATOR CONFIGURATION

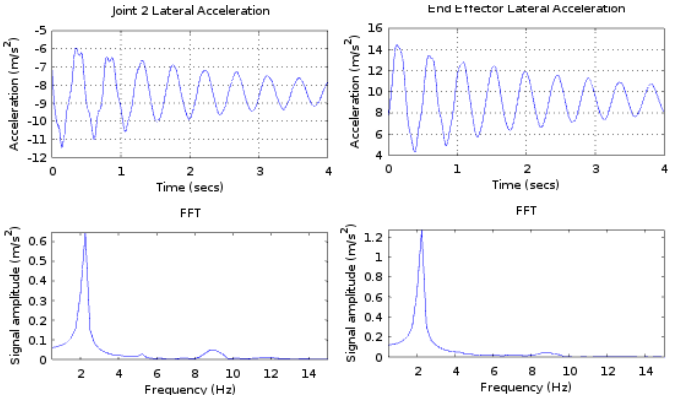

FIGURE 14: LATERAL ACCELERATION AND FAST FOURIER TRANSFORM OF RESIDUAL VIBRATION FOR FINAL MANIPULATOR CONFIGURATION

changes in speed, spaced at empirically determined natural periods. The inbuilt Hebi position controller was used to provide a comparison of naive point to point motion.

Impulse Shaping For the purpose of forming the velocity profile for open loop input shaped control, the manipulator was brought rapidly to a stop at both the initial and final configurations in order to determine the natural frequency for each set of joint angles. Figure 13 shows the lateral acceleration in the plane of motion for Joint 2 and the end effector in the initial configuration of $(\theta_1, \theta_2) = (-\pi/4, \pi/4)$, along with a Fast Fourier Transform of the residual vibration. The first mode occurs at 2.25Hz, with a second mode of much smaller amplitude at 10Hz seen mostly in Joint 2. Natural frequencies were then evaluated at the final configuration of $(\theta_1, \theta_2) = (\pi/4, -\pi/4)$, to determine if timing of velocity steps would need to differ significantly between acceleration and deceleration.

As seen in Fig. 14, the first mode remained at 2.25Hz while the second reduced slightly to 9Hz. Given that input shaping was initially only going to be applied to the first mode this meant that velocity steps could be mirrored between acceleration and deceleration, with a spacing of half the period of the first mode at 222ms.

$$(A_1, A_2) = \left(\frac{1}{1+K}, \frac{K}{1+K}\right) \tag{3}$$

$$K = e^{\frac{-\zeta\omega}{\sqrt{1-\zeta^2}}} \tag{4}$$

Simulations did not include damping and so the amplitude of the two impulses in ZV shaped acceleration being employed in this experiment were of equal magnitude. As this is not the case in a real system the relative amplitude of each acceleration impulse is a function of the system damping for each respective mode as seen in Eq. 3, where K is a function of damping factor and natural frequency as in Eq. 4.

Damping factor was determined from the change in amplitude of successive peaks of the residual vibration at the initial and final configurations to be -0.0211 and -0.0254 respectively. This produced an average amplitude factor between them of $K = 0.903$.

Measurement of Residual Vibration As the joint elasticity within the actuators was of much lower effective stiffness than the aluminum links, the dual encoders of the Hebi motors that measured internal deflection allowed inference of total system vibration. As the apparatus lacked the ability to resolve the absolute position of the end effector, the robustness of positioning against changes in system parameters could not be ascertained, but the main interest was on the amplitude of residual vibration and jerk.

Fig. 15 shows the input shaped velocity profiles for each joint during the motion, after the Hebi PI velocity control gains were tuned to improve the step response. Delays between velocity steps and relative amplitudes were tuned to match the previously determined values.

A comparison of the motor output angles from the first joint between the naive rapid and input shaped trajectories can be seen in Fig. 16. The right image illustrates the reduction in amplitude of residual vibration achieved by the input shaped trajectory, at only 27% of the amplitude from the naive rapid motion. The shaped impulses or velocity step changes are visible in the input shaped response in the left figure.

While the amplitude of residual vibration is reduced, the input shaped trajectory produces a longer burst of transient lateral acceleration in the end effector, as seen in Fig. 17, which would

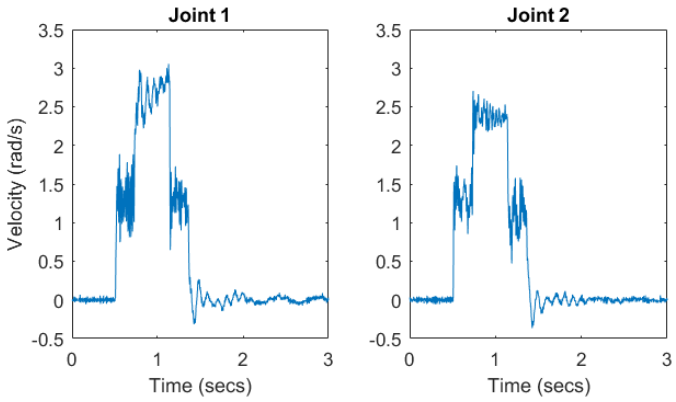

FIGURE 15: VELOCITY PROFILE WITH ACCELERATION AND DECELERATION IMPULSES FOR JOINT 1 AND JOINT 2 OF THE MANIPULATOR DURING THE INPUT SHAPED MOTION

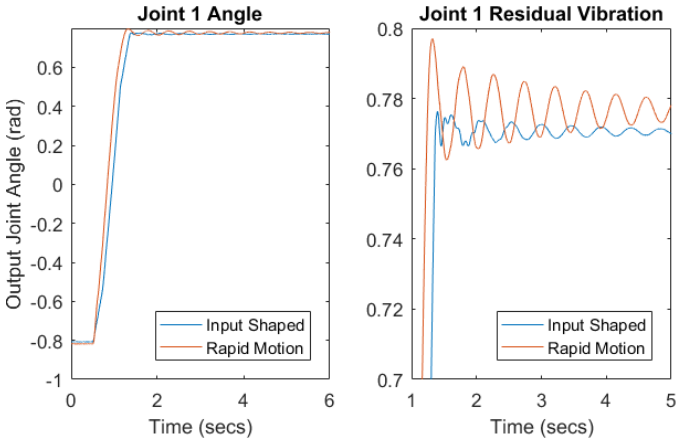

FIGURE 16: JOINT 1 MOTOR OUTPUT ANGLE WITH BOTH NAIVE RAPID AND INPUT SHAPED TRAJECTORIES

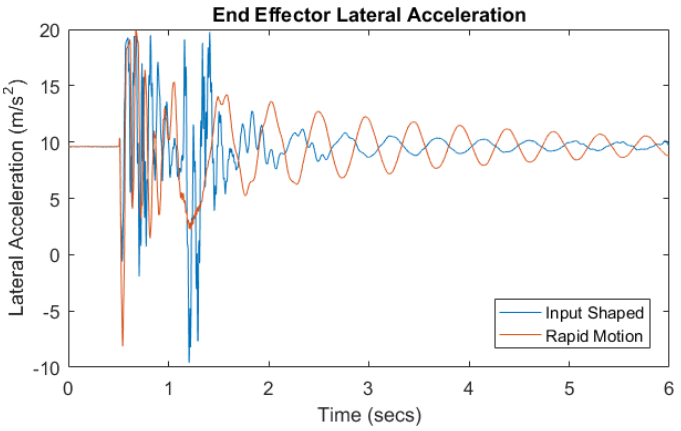

FIGURE 17: LATERAL ACCELERATION OF MANIPULATOR END EFFECTOR WHICH IS HELD HORIZONTAL DURING MOTION WITH BOTH NAIVE RAPID AND INPUT SHAPED TRAJECTORIES

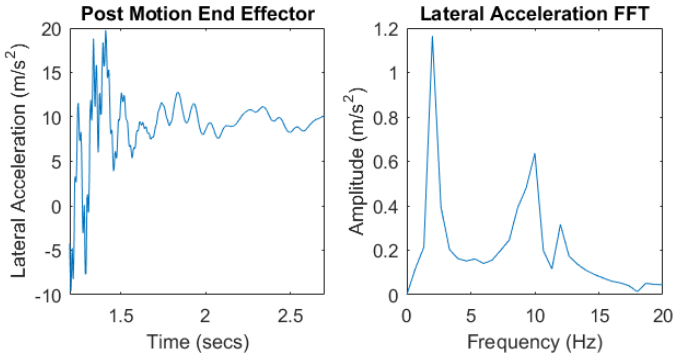

FIGURE 18: CLOSE UP (LEFT) AND FAST FOURIER TRANSFORM (RIGHT) OF END EFFECTOR LATERAL ACCELERATION AFTER MOTION, ILLUSTRATING INCREASED AMPLITUDE OF SECOND MODE

in effect increase the jerk experienced by a payload during the motion. An FFT reveals that this lengthened burst of transient acceleration is in fact caused by the second mode being excited by each impulse in the input shaped trajectory, as seen in Fig. 18.

This indicates that while input shaping for the first mode has shown a significant decrease in the position amplitude of residual vibration, the second mode will likely also need to be addressed so as to limit jerk experienced by a payload.

Second Mode Shaping In order to shape velocity profiles that allow cancellation of the second natural mode the control system must be capable of issuing updates at sufficient speed to create impulses spaced by half the period of the mode. For this reason it was necessary to quantify the achievable update rate and the jitter associated with the TCP/IP connection. This was achieved through use of an additional Hebi API command named 'sendCommandWithAcknowledgement', which ensures transmission of each command within the control cycle, giving a fair representation of transmission time. Figure 19 demonstrates that the typical period between command cycles averages around 5ms, which could be sufficient to achieve the 50ms impulse spacing required for the second mode if the velocity controller were able to track the desired profile reliably.

It appears, however, that given the internal Hebi controller's use of the post series elasticity angle as the control output, the bandwidth of the controller is not sufficient to apply velocity

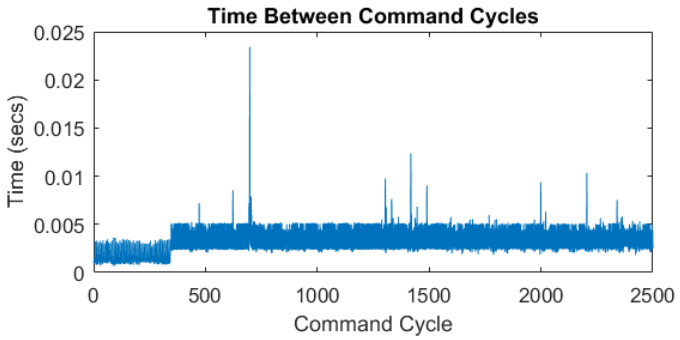

FIGURE 19: DURATION BETWEEN SUCCESSIVE COMMAND CYCLES WHEN USING THE 'sendcommandwithacknowledgement' FUNCTION USED TO DETERMINE CONTROL BANDWIDTH

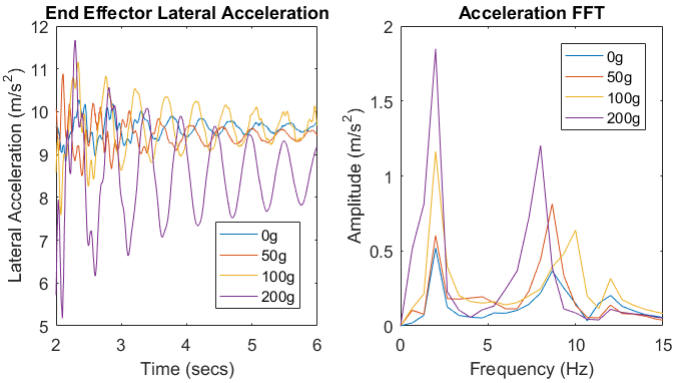

FIGURE 20: CHANGE IN RESIDUAL VIBRATION OF END EFFECTOR AS A RESULT OF INCREASED PAYLOAD MASS

steps in these small increments and time steps. This application would be better suited to a real time controller applied to a high reduction motor without an internal series elasticity to account for. Acceleration impulses could then more accurately be produced, which would be designed to account for all external compliance.

Robustness As in simulation, it was of interest to determine how the response to the open loop control is affected by changes in system parameters such as payload mass. For this purpose a range of calibration weights were affixed to the third Hebi motor to act as a disturbance factor in the payload mass.

Final positioning error was significant even for small added payload due to the internal Hebi velocity controller producing a lower output speed in response to the increased mass, resulting in a reduced motion. The focus of the robustness analysis was therefore on the amplitude of residual oscillation after a change in expected payload mass. Figure 20 shows the increase in amplitude of both the first and second mode that occurs when system mass is increased, which has the effect of changing the natural period and therefore causing the tuned spacing of acceleration impulses to no longer fully cancel residual vibrations.

As seen in simulation, the robustness of the purely open loop input shaped response could be improved by reducing velocity sufficiently to include three impulses for both acceleration and deceleration, though this would of course render the trajectory much slower. Application of an LQR feedback controller would also allow changes in system parameters to be more easily accounted for, however, as with the implementation of command shaping for the second mode, this would likely require the use of a realtime motor controller as the Hebi internal controls only act on the post spring angle, and are limited in computer control bandwidth by TCP/IP and a non-realtime OS.

CONCLUSION

A model predictive controller based on a linearized model of a flexible two-link manipulator has been implemented in simulation, and the stability of the controller found to be related to the number of system natural periods contained within the prediction horizon of the MPC. This was compared to the performance of open loop command shaped joint trajectories, which produced superior rapid point to point tracking compared to MPC but were not robust to variations in parameters with significant residual vibration, as is expected of open loop control.

The addition to the command shaping of feedback control in the form of LQR proved effective in reducing residual vibration but introduced steady state error in end effector position as the tracked states were joint angle rather than tip location. This could be improved upon with adaptive control to inform LQR parameters of changes in payload mass or link compliance.

An experimental testbed was developed to evaluate the rapid tracking performance of the open loop command shaped control, which demonstrated reduced amplitude of the first mode while increasing that of the second. Velocity profiles capable of accounting for the second mode were found to be beyond the temporal resolution of the chosen control system, though proved effective in simulation. Increases in residual vibration with payload variation were also in keeping with simulated results.

Command shaping has been demonstrated as a more effective control scheme for rapid point to point motion of a flexible two-link manipulator when system parameters are well known, but is inferior to model predictive control in regard to vibration reduction when values such as payload mass are variable. This result may change with the addition of adaptive control to the open loop command shaping technique.

REFERENCES

[1] Mankins, J. C., 2002. "A technical overview of the "suntower" solar power satellite concept". *Acta Astronautica,* ***50***(6), pp. 369 – 377.

[2] Trauger, J. T., and Traub, W. A., 2007. "A laboratory demonstration of the capability to image an earth-like extrasolar planet". *Nature,* ***446***(7137), pp. 771–773.

[3] Hogstrom, K., Backes, P., Burdick, J., Kennedy, B., Kim, J., Lee, N., Malakhova, G., Mukherjee, R., Pellegrino, S., and Wu, Y., 2014. "A robotically-assembled 100-meter space telescope". In International Astronautical Congress, International Astronautical Federation.

[4] Scott, M. A., Gilbert, M. G., and Demeo, M. E., 1993. "Active vibration damping of the space shuttle remote manipulator system". *Journal of guidance, control, and dynamics,* ***16***(2), pp. 275–280.

[5] Mukherjee, R. M., and Anderson, K. S., 2007. "A logarithmic complexity divide-and-conquer algorithm for multiflexible articulated body dynamics". *Journal of computational and nonlinear dynamics,* ***2***(1), pp. 10–21.

[6] Cannon, R. H., and Schmitz, E., 1984. "Initial experiments on the end-point control of a flexible one-link robot". *The International Journal of Robotics Research,* ***3***(3), pp. 62–75.

[7] Bricout, J., Debus, J., and Micheau, P., 1990. "A finite element model for the dynamics of flexible manipulators". *Mechanism and Machine Theory,* ***25***(1), pp. 119–128.

[8] Zhu, G., Ge, S. S., and Lee, T. H., 1999. "Simulation studies of tip tracking control of a single-link flexible robot based on a lumped model". *Robotica,* ***17***(1), pp. 71–78.

[9] Dwivedy, S. K., and Eberhard, P., 2006. "Dynamic analysis of flexible manipulators, a literature review". *Mechanism and machine theory,* ***41***(7), pp. 749–777.

[10] Karkkainen, P., 1985. "Compensation manipulator flexibility effects by modal space techniques". In Robotics and Automation. Proceedings. 1985 IEEE International Conference on, Vol. 2, IEEE, pp. 972–977.

[11] Theodore, R. J., and Ghosal, A., 1995. "Comparison of the assumed modes and finite element models for flexible multilink manipulators". *The International journal of robotics research,* ***14***(2), pp. 91–111.

[12] Ficola, A., Fravolini, M. L., and La Cava, M., 2001. "On control of flexible robots". In *Ramsete*. Springer, pp. 103–120.

[13] Boscariol, P., Gasparetto, A., and Zanotto, V., 2010. "Model predictive control of a flexible links mechanism". *Journal of Intelligent & Robotic Systems,* ***58***(2), pp. 125–147.

[14] Singer, N. C., and Seering, W. P., 1990. "Preshaping command inputs to reduce system vibration". *Journal of Dynamic Systems, Measurement, and Control,* ***112***(1), pp. 76–82.

[15] Mohamed, Z., and Tokhi, M., 2002. "Vibration control of a single-link flexible manipulator using command shaping techniques". *Proceedings of the Institution of Mechanical Engineers, Part I: Journal of Systems and Control Engineering,* ***216***(2), pp. 191–210.

[16] Benosman, M., and Le Vey, G., 2004. "Control of flexible manipulators: A survey". *Robotica,* ***22***(05), pp. 533–545.

[17] Romano, M., Agrawal, B. N., and Bernelli-Zazzera, F., 2002. "Experiments on command shaping control of a manipulator with flexible links". *Journal of Guidance, Control, and Dynamics,* ***25***(2), pp. 232–239.

[18] Khorrami, F., Jain, S., and Tzes, A., 1995. "Experimental results on adaptive nonlinear control and input preshaping for multi-link flexible manipulators". *Automatica,* ***31***(1), pp. 83–97.

[19] Singhose, W., 2009. "Command shaping for flexible systems: A review of the first 50 years". *International Journal of Precision Engineering and Manufacturing,* ***10***(4), pp. 153–168.

ACKNOWLEDGMENT

The research described in this paper was carried out by the Jet Propulsion Laboratory, California Institute of Technology, under a contract with the National Aeronautic and Space Administration.